2020 IEEE/RSJ International Conference on Intelligent Robots and Systems (IROS)
October 25-29, 2020, Las Vegas, NV, USA (Virtual)

Quadrupedal Robotic Walking on Sloped Terrains via Exact Decomposition into Coupled Bipedal Robots

Wen-Loong Ma[1], Noel Csomay-Shanklin[2] and Aaron D. Ames[1,2]

***Abstract*— Can we design motion primitives for complex legged systems uniformly for different terrain types without neglecting modeling details? This paper presents a method for rapidly generating quadrupedal locomotion on sloped terrains—from modeling to gait generation, to hardware demonstration. At the core of this approach is the observation that a quadrupedal robot can be exactly decomposed into coupled bipedal robots. Formally, this is represented through the framework of coupled control systems, wherein isolated subsystems interact through coupling constraints. We demonstrate this concept in the context of quadrupeds and use it to reduce the gait planning problem for uneven terrains to bipedal walking generation via hybrid zero dynamics. This reduction method allows for the formulation of a nonlinear optimization problem that leverages low-dimensional bipedal representations to generate dynamic walking gaits on slopes for the full-order quadrupedal robot dynamics. The result is the ability to rapidly generate quadrupedal walking gaits on a variety of slopes. We demonstrate these walking behaviors on the Vision 60 quadrupedal robot; in simulation, via walking on a range of sloped terrains of $13^\circ, 15^\circ, 20^\circ, 25^\circ$, and, experimentally, through the successful locomotion of 13° and $20^\circ \sim 25^\circ$ sloped outdoor grasslands.**

I. Introduction

Numerous examples of successful bipedal locomotion, including but not limited to [1], [2], [3], have been witnessed in the past decade. However, limited formal results have shown the capability of these bipedal systems robustly traversing outdoor environments such as stairs, slopes, stepping stones, etc. Due to the benefits of the additional legs able to stabilize the robot, quadrupedal robotic locomotion has demonstrated prominent agility and robustness on rough terrains, such as [4], [5], [6], [7], and, some of the works such as [8] has even shown successful locomotion on sloped terrains. However, state-of-the-art approaches for the control of quadrupeds largely utilized reduced models to mitigate the complexity of the full-body dynamics of quadrupedal robots. Such reductions include the linear inverted pendulum model [9], the virtual-leg principle [10], massless leg assumption [6], planar model simplification [7], and neglecting the impacts for the gait design. These methods have been demonstrated to be effective in practice, but the simplified models come with a tradeoff of scalability. A well tuned controller for a specific robot on a definite terrain type might not be optimal for another scenario. Often, when the terrain dynamics vary, intensive parameter tuning could be needed. We are interested in generating agile quadrupedal locomotion efficiently and consistently that can overcome outdoor sloped terrains that requires little to no tuning.

This work was supported by NSF grant 1924526 and 1923239.

1 is with the department of Mechanical Engineering, 2 is with the department of Control+Dynamical Systems, California Institute of Technology, Pasadena, CA, USA. {wma, noelcs, ames}@caltech.edu.

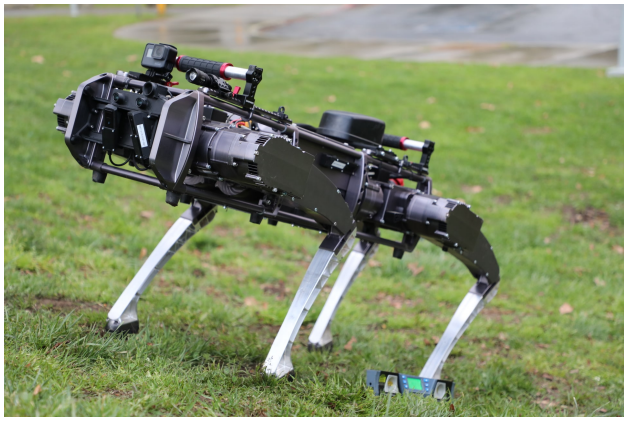

Fig. 1: The Vision 60 quadrupedal robot (V3.9) standing on a $20^\circ \sim 25^\circ$ sloped lawn.

At the theoretical level, the Hybrid Zero Dynamics (HZD) framework that was built to provide stability guarantees to bipedal locomotion (see [11]) has shown great scalability spanning various dynamic behaviors and robotic platforms such as: multi-contact walking [12], running [13], slippery surface walking [14], and prosthesis locomotion [15]. Aimed at bridging the gap between the formal analysis of bipedal walking and practicality of quadrupedal locomotion, previous work [16] decomposes the full-body dynamics of a quadrupedal robot into two coupled bipedal robots, and [17] generalize it to periodic orbit generation for coupled control systems (CCSs). By generating walking gaits for a bipedal robot subject to coupling conditions, rapid gait generation was achieved, and robust locomotion on flat ground was obtained on a 26 kg robot, the Vision 60 v3.2 quadruped. A related methodology was also used to produce collaboration between quadrupedal robots, as demonstrated in [18].

Taking advantage of the benefits of the aforementioned design methodology, in this paper we further scale the CCS method to locomotion on slopped terrains with a heavier and bigger quadrupedal platform. We achieve this by modifying the terrain dynamics and feasibility conditions on the basis of the CCS method in [17], which allows us to exactly decompose the full-body dynamics of a quadrupedal robot into the coupled dynamics of two bipedal robots. Hence, model simplification is avoided while fast computational speed is obtained. The result is the 44 kg quadrupedal robot — Vision 60 v3.9, walking on a range of sloped terrains of $13^\circ, 15^\circ, 20^\circ, 25^\circ$ in a physics engine — RaiSim [19],

and experimental walking in sloped grasslands at 13° and $20^\circ \sim 25^\circ$. This is done with only one static parameter—the slope of the terrain—that is specified by user. In addition, the optimization setup and control law is consistent across all tests in both simulation and experiment with no additional gain tuning required by the user. This seamlessly transition from gait design to implementation suggests a new approach towards designing quadrupedal locomotion for outdoor environments.

This paper is organized as follows: Sec. II presents the decomposed dynamics of the quadrupedal robot on sloped terrains, and by using the notion of coupled control systems, we isolate the bipedal dynamics from quadrupeds. Sec. III then finds the periodic solution of the isolated bipedal dynamics with an optimization algorithm, which is then reconstructed to quadrupedal gaits on slopes. In Sec. IV, we validate the dynamic stability of five optimal gaits and their controllers on different sloped terrains of $0^\circ, 13^\circ, 15^\circ, 20^\circ, 25^\circ$ in RaiSim and outdoor sloped grasslands. We finish with conclusions and future plans in Sec. V.

II. Decomposed Dynamics on Sloped Terrains

In this section, we systematically decompose the dynamics of a quadrupedal walking system on slopes into two coupled bipedal robots. Following the general method of Coupled Control System (CCS) in [17], we modify the model-based controllers that render the zero dynamics manifold invariant while eliminating the dependence on the other bipedal subsystem through the coupling condition, in the context of sloped walking and rigid-body connection.

A. Coupled Control Systems (CSS)

The dynamics of a coupled control system are given by

$$\mathcal{C}_{\mathcal{C}} \triangleq \begin{cases} \dot{x}_i = f_i(x_i, z_i) + g_i(x_i, z_i)u_i + \breve{g}_e(x_i, z_i, z_j)\lambda_e \\ \dot{z}_i = p_i(x_i, z_i) + q_i(x_i, z_i)u_i + \breve{q}_e(x_i, z_i, z_j)\lambda_e \\ \text{s.t.} \quad c_e(z_i, z_j) = z_i - z_j \equiv 0 \\ \qquad \lambda_e = -\lambda_{\bar{e}} \end{cases} \tag{1}$$

for all $i \in \mathcal{N}$, where $\mathcal{N} = \{1, 2\}$ is a set of subsystem indices and $e \triangleq (i, j) \in \mathcal{E}$ is a set of edges representing the connection relation between two subsystems; $\mathcal{X} = \mathcal{X}_1 \times \mathcal{X}_2$ is a set of *internal states*, with coordinates $x = (x_1, x_2) \in \mathcal{X}$; $\mathcal{Z} = \mathcal{Z}_1 \times \mathcal{Z}_2$ is a set of *coupled states*, with coordinates $z = (z_1, z_2) \in \mathcal{Z}$; $\mathcal{U} = \mathcal{U}_1 \times \mathcal{U}_2$ is a set of *admissible inputs*, with coordinates $u = (u_1, u_2) \in \mathcal{U}$; $C = \{c_e\}_{e=(i,j)\in\mathcal{E}} \equiv 0$ is a *coupling constraint* between the two subsystems.

We now can design the control law $u_j^{\mathbf{Z}}$ that renders the zero dynamics manifold of the j^{th} subsystem $\mathbf{Z}_j \triangleq \{(x, z) \in \mathcal{X} \times \mathcal{Z} \mid x_j \equiv 0\}$ invariant, i.e., $u_j^{\mathbf{Z}}$ satisfies

$$0 \equiv f_j^{\mathbf{Z}}(0, z) + g_j^{\mathbf{Z}}(0, z)u_j^{\mathbf{Z}} + g_j(0, z_j)\left(u_j^{\mathbf{Z}}(0, z; u_i) - u_i\right).$$

Following [17], given a coupling condition as

$$\lambda_e^{\mathbf{Z}}(x_i, z; u_i) = A_e^{\mathbf{Z}}(x_i, z)u_i + b_e^{\mathbf{Z}}(x_i, z), \tag{2}$$

we can obtain the the i^{th} ***control subsystem (CSub)*** associated with the CCS $\mathcal{C}_{\mathcal{C}}$ as:

$$\mathcal{C}_i^{\mathbf{Z}} \triangleq \begin{cases} \dot{x}_i = f_i^{\mathbf{Z}}(x_i, z) + g_i^{\mathbf{Z}}(x_i, z)u_i \\ \dot{z}_i = p_i^{\mathbf{Z}}(x_i, z) + q_i^{\mathbf{Z}}(x_i, z)u_i \\ \dot{z}_j = p_j^{\mathbf{Z}}(x_i, z) + q_j^{\mathbf{Z}}(x_i, z)u_i \end{cases} \tag{3}$$

where,

$$\begin{aligned} f_i^{\mathbf{Z}}(x_i, z) &= f_i(x_i, z_i) + \breve{g}_e(x_i, z_i, z_j)b_e^{\mathbf{Z}}(x_i, z), \\ g_i^{\mathbf{Z}}(x_i, z) &= g_i(x_i, z_i) + \breve{g}_e(x_i, z_i, z_j)A_e^{\mathbf{Z}}(x_i, z), \\ p_i^{\mathbf{Z}}(x_i, z) &= p_i(x_i, z_i) + \breve{q}_e(x_i, z_i, z_j)b_e^{\mathbf{Z}}(x_i, z), \\ q_i^{\mathbf{Z}}(x_i, z) &= q_i(x_i, z_i) + \breve{q}_e(x_i, z_i, z_j)A_e^{\mathbf{Z}}(x_i, z). \end{aligned}$$

As a special case of [17], we note the particular coupling structure —rigid-body connection— of the problem of interests in this paper:

$$c_e(z_i, z_j) = z_i - z_j \equiv 0,$$

i.e., all of the coupled states are shared through each subsystem. Hence, $p_j^{\mathbf{Z}} = p_i^{\mathbf{Z}}, q_j^{\mathbf{Z}} = q_i^{\mathbf{Z}}$ further simplifying the dynamics in (3). According to Theorem 1 of [17], when applying a controller $u_i = u_i(x_i, z)$ to $\mathcal{C}_i^{\mathbf{Z}}$, the solution to the resultant dynamical system can be reconstructed to the solution to $\mathcal{C}_{\mathcal{C}}$. This allows us to exactly reduce the trajectory optimization problem of (1) into that of (3).

B. CCS formulation for quadrupeds

We now instantiate this idea to quadrupedal walking on slopes. The robot of interests — Vision 60 v3.9 as shown in Fig. 1 — is composed of 13 links: a *body* link and four *limb* links, each of which has three sublinks — the hip, thigh and calf. As given by (1), we write the full-body dynamics of a quadruped as coupled control system of two bipeds. A set of semi-explicit differential algebraic equations are given by

$$\begin{cases} D_i\ddot{q}_i + H_i = J_i^\top F_i + B_i u_i + J_e^\top \lambda_e \\ J_i\ddot{q}_i + \dot{J}_i\dot{q}_i = 0 \\ \text{s.t.} \quad c_e(\xi_i, \xi_j) = \xi_i - \xi_j \equiv 0, \ \lambda_e = -\lambda_{\bar{e}} \end{cases} \tag{4}$$

defined for all $i \in \mathcal{N}$, with the following notations: $\mathcal{N} = \{\text{f}, \text{r}\}$ is a set of nodes labeling the front and rear bipeds and $\mathcal{E} = \{e = (\text{f}, \text{r}), \bar{e} = (\text{r}, \text{f})\}$ labels their edges; the configuration coordinates are $q_{\text{f}} = (\xi_{\text{f}}^\top, \theta_{\text{L}_2}^\top, \theta_{\text{L}_0}^\top)^\top \in \mathcal{Q}_{\text{f}}$, $q_{\text{r}} = (\xi_{\text{r}}^\top, \theta_{\text{L}_1}^\top, \theta_{\text{L}_3}^\top)^\top \in \mathcal{Q}_{\text{r}}$; the "base" coordinates $\xi_i \in \mathbb{R}^3 \times \text{SO}(3)$ represents the Cartesian position and orientation of the *body* link; the "shape" coordinates $\theta_{L_*} \in \mathbb{R}^3$ represents the three joint angles on the leg L_*. Therefore, we have $\mathcal{Q}_i \subset \mathbb{R}^3 \times \text{SO}(3) \times \mathbb{R}^6$, and the total degrees of freedom for each biped is $n = 3 + 3 + 6 = 12$. Since all of the shape coordinates are actuated by motors, the inputs are $u_i \in \mathcal{U} \subset \mathbb{R}^6$; Finally, $D_i(q_i) \in \mathbb{R}^{n\times n}$ is the inertia-mass matrix, $H_i(q_i) \in \mathbb{R}^n$ is the drift vector containing the Coriolis, centrifugal, and gravity terms. The contact condition is represented by a holonomic constraints $h_i(q)$ with Jacobian matrix $J_i \triangleq \partial h_i(q_i)/\partial q_i$, with a ground reaction force $F_i \in \mathbb{R}^3$.

To simplify notations, we remark that the first two equations of (4), which represents the bipedal dynamics subject

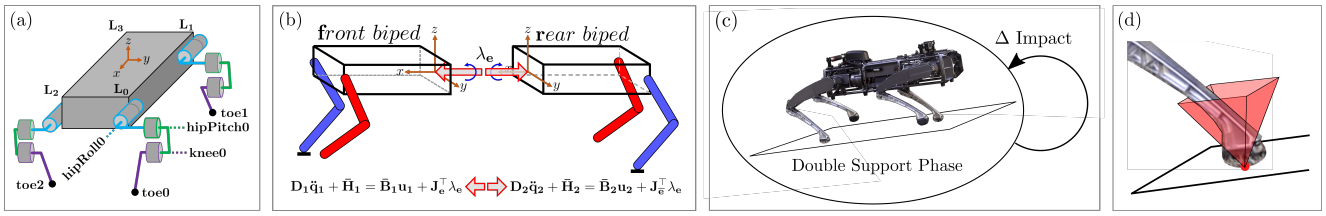

Fig. 2: (a) the configuration coordinates of the full-body dynamics of a quadruped; (b) the decomposed dynamics of quadruped into two coupled bipedal robots; (c) the cyclic directed graph for the multi-domain hybrid dynamics on sloped terrain; (d) friction cone (pyramid) condition on some sloped terrain.

to some holonomic constraints $h_i(q_i) \equiv 0$, can be folded into a shorter form by solving F_i, which yields

$$\begin{cases} D_i\ddot{q}_i + \bar{H}_i = \bar{B}_i u_i + \bar{J}_e^\top \lambda_e \\ \text{s.t.} \quad c_e(\xi_i, \xi_j) = \xi_i - \xi_j \equiv 0, \ \lambda_e = -\lambda_{\bar{e}}. \end{cases} \tag{5}$$

The control target is to drive the following outputs:

$$y_i(q_i, \alpha_i, t) \triangleq \theta_i - y_i^d(\tau(t), \alpha_i) \tag{6}$$

to zero, where θ_i represents all of the shape coordinates of the i^{th} biped, $\tau(t) \in [0, 1]$ is the parameterized time, and $\alpha_i \in \mathbb{R}^{6\times 6}$ parameterizes the desired outputs y_i^d that is designed by a CCS-optimization method in Sec. III. Note that $(y^\top, \dot{y}^\top)^\top$ are the internal states x as appeared in (3). Since we wish to design a *symmetric ambling motion* on sloped terrains, $\alpha_{\text{r}} = \mathcal{M}\alpha_{\text{f}}$ is implied, with the matrix $\mathcal{M}$ representing a mirroring relation between the front and rear bipedal subsystems. Specifically, the desired behaviors of leg 1 and 3 mirrors those of leg 2 and 0, correspondingly.

Coupling Relations for Robotic Systems. Following the previous construction, we can have the explicit form of the controller $u_j^{\mathbf{Z}}$ that renders zero dynamics manifold $\mathbf{Z}_j$ invariant and the coupling condition in (2) as

$$\begin{bmatrix} u_j^{\mathbf{Z}}(x_i, z; u_i; t) \\ \lambda_{\bar{e}}^{\mathbf{Z}}(x_i, z; u_i; t) \end{bmatrix} = \begin{bmatrix} J_{y_j} D_j^{-1} \bar{B}_j & -J_{y_j} D_j^{-1} \bar{J}_{\bar{e}}^\top \\ J_{\xi_j} D_j^{-1} \bar{B}_j & -J_{\xi_j} D_j^{-1} \bar{J}_{\bar{e}}^\top - J_{\xi_i} D_i^{-1} \bar{J}_e^\top \end{bmatrix}^{-1}$$
$$\Big(\begin{bmatrix} \ddot{y}^d - \dot{J}_{y_j}\dot{q}_j - J_{y_j} D_i^{-1} \bar{H}_j \\ -J_{\xi_i} D_i^{-1} \bar{H}_i + J_{\xi_j} D_j^{-1} \bar{H}_j \end{bmatrix} + \begin{bmatrix} 0 \\ J_{\xi_i} D_i^{-1} \bar{B}_i \end{bmatrix} u_i \Big) \tag{7}$$

where $J_{y_i} = \partial y_i / \partial q_i$, $J_{\xi_i} = \partial q_i / \partial \xi_i$. Note that we suppressed the the dependence on x_i, z, t for notation simplicity. From this, we can obtain the CSub $\mathcal{C}_i^{\mathbf{Z}}$, as in (3).

Isolating Bipeds from Quadrupeds. The framework of CCS allows for the isolation of a subsystem. However, the matrix inversion in (7) can compromise the computational performance. Hence, we take these ideas one step further to obtain bipeds that are the isolated subsystems associated with quadrupeds and include slack variables that are beneficial for gait generation. Operating on the forward invariant zero dynamics manifold $\mathbf{Z}_j$ yields $y_j \equiv 0 \Rightarrow \theta_j^{\mathbf{Z}} \equiv y^d(t, \alpha_j)$, and

$$\begin{aligned} q_j^{\mathbf{Z}} &\equiv (\xi_j^\top, (y^d(t, \alpha_j))^\top)^\top, \\ \Rightarrow \ \dot{q}_j^{\mathbf{Z}} &= (\dot{\xi}_j^\top, (\dot{y}^d(t, \alpha_j))^\top)^\top, \\ \Rightarrow \ \ddot{q}_j^{\mathbf{Z}} &= (\ddot{\xi}_j^\top, (\ddot{y}^d(t, \alpha_j))^\top)^\top. \end{aligned}$$

In another word, if $u_j^{\mathbf{Z},\lambda}$ exists and is applied, the bipedal dynamics subject to the coupling wrench are equivalent to:

$$\begin{cases} D_j\ddot{q}_j^{\mathbf{Z}} + H_j = J_j^\top F_j + B_j u_j^{\mathbf{Z}} + J_{\bar{e}}^\top \lambda_{\bar{e}} & (8) \\ J_j\ddot{q}_j^{\mathbf{Z}} + \dot{J}_j\dot{q}_j^{\mathbf{Z}} = 0 & (9) \end{cases}$$

where for simplicity we have suppressed the arguments of $D_j(q_j^{\mathbf{Z}})$, $J_j(q_j^{\mathbf{Z}})$, and $H_j(q_j^{\mathbf{Z}}, \dot{q}_j^{\mathbf{Z}})$. We now leverage a specific structure of rigid-body dynamics using the floating base convention [20]: $B_j u_j + J_{\bar{e}}^\top \lambda_{\bar{e}} = (\lambda_{\bar{e}}^\top, u_j^\top)^\top$. Utilizing this, the first 6 rows of (8) and (9) yields the following:

$$\mathcal{R}_{\mathcal{B}}^{\mathbf{Z}_j} \triangleq \begin{cases} \hat{D}_j\ddot{q}_j^{\mathbf{Z}} + \hat{H}_j = \hat{J}_j^\top F_j + \lambda_{\bar{e}} \\ J_j\ddot{q}_j^{\mathbf{Z}} + \dot{J}_j\dot{q}_j^{\mathbf{Z}} = 0 \end{cases} \tag{10}$$

where, $\hat{\square}$ are the first 6 rows of a variable. Hence, $\mathcal{R}_{\mathcal{B}}^{\mathbf{Z}_j}$ represents the dynamics of the j^{th} subsystem on $\mathbf{Z}_j$ with a slack variable F_j, which can be uniquely determined.

C. Hybrid dynamics on slopes

We consider the quadrupedal locomotion as a hybrid dynamical system, which is an alternating sequence of continuous- and discrete-time dynamics. The directed graph is illustrated in Fig. 2 (d). More details of hybrid modeling for bipedal and quadrupedal locomotion can be found in [20], [21]. Here, we elaborate the problem formulation for walking on slopes using the isolated bipedal dynamics in (10). Note that we only consider sloped terrains with a pitch angle of $\phi \in \mathbb{R}$ in the world's frame in this paper.

Guard condition and discrete dynamics on slopes. For the symmetric ambling motion, the diagonal toes of the quadrupedal robot stay on the ground while the other two toes are swing in the air. This means each bipedal robot has one toe-foot in contact with the ground. Concretely, the Cartesian position of the stance toe remains zero, i.e. $h_s(q_i) \equiv 0$. This contact constraint is enforced by a ground reaction force $F_i \in \mathbb{R}^3$, where $i \in \{\text{f}, \text{r}\}$. We additionally denote the Cartesian position of the nonstance toe along x, z directions as $h_{ns}^x(q_{\text{f}}), h_{ns}^z(q_{\text{f}}) \in \mathbb{R}$. The nonstance foot's height on the slope is then given by

$$\hat{h}_{ns}(q_i) = h_{ns}^z(q_i)\sin\phi - h_{ns}^x(q_i)\cos\phi.$$

Hence we can define the single-support domain for bipedal dynamics (10) as:

$$\mathcal{D}_i \triangleq \{(q_i, \dot{q}_i) \in \mathcal{Q}_i \times T\mathcal{Q}_i \mid h_s(q_i) = 0, \hat{h}_{ns}(q_i) \geq 0\}.$$

The guard is then defined on the edge of the domain $\mathcal{D}_i$ as $\mathcal{S}_i \triangleq \{(q_i, \dot{q}_i) \in \mathcal{Q}_i \times T\mathcal{Q}_i \mid h_s(q_i) = \hat{h}_{ns}(q_i) = 0, \dot{\hat{h}}_{ns}(q_i, \dot{q}_i) < 0\}$, on which we define the discrete dynamics that represents plastic impacts (see equation (20) in [16]) at the event that nonstance toe touches down.

The friction cone condition on slopes. The feasibility conditions $\mathcal{A}_i(F_i) \geq 0$ are enforced to guarantee the solutions to

the dynamics is physically realizable. In particular, we have the friction pyramid condition on sloped terrains as:

$$\mathcal{A}_i(F_i) \triangleq \begin{cases} F_i^z \cos\phi - F_i^x \sin\phi \\ \mu(F_i^z \sin\phi + F_i^x \cos\phi) - |F_i^z \cos\phi - F_i^x \sin\phi| \\ \mu(F_i^z \sin\phi + F_i^x \cos\phi) - |F_i^y| \end{cases} \tag{11}$$

where μ is the coefficient of dynamic friction of the ground. It is worth noting the feasibility formulation (11) is more restrictive for walking on sloped terrains than walking on stairs or level ground.

III. CCS Optimization on Slopes

Having established the isolated dynamics as bipedal robots from the full-body dynamics of a quadrupedal robot, we use optimization to find a periodic solution to the robotic dynamics, representing a quadrupedal behavior — ambling. The goal is to design trajectories of the front bipeds that are subject to the coupling constraints $c_e(z) \equiv 0$. The quadrupedal ambling behavior on sloped terrains is then reconstructed from the bipedal trajectories.

Dynamic collocation constraints. In this paper, we utilize a direct collocation based method and the toolbox FROST [22] to mitigate the computational complexity finding the solutions. Direct collocation (see [23]) is an implicit Runge–Kutta method for numerically approximating the exact solution of a dynamical system. Given the evenly discretized time $\{t^\kappa\}$ with indices $\kappa = 0, 1, ...\mathrm{K}$, we pose the dynamic equations as a set of equality constraints on every node κ, and then use Hermite-Simpson method to interpolate the states in the middle of every two nodes. If the interpolated state also satisfies the dynamical equations, i.e., the collocation constraints are satisfied, the numerical solution has been found for all $t \in [0, T]$. Here, the dynamic constraints are given by (4) for $i \in \mathcal{N}$ and (10) for $j \in \mathcal{N} \neq i$, which is then posed correspondingly as equality constraints on nodes $\kappa \in (0, 1, \ldots, \mathrm{K})$, referred as the ***dynamic collocation constraints***. More details can be found in [17].

Periodic constraints. A stable periodic motion can be expanded to the infinite time horizon. Hence, our goal is to find a periodic solution to the dynamical system. To accomplish this, we use an equality constraint in the form of

$$b(q_i^0, \dot{q}_i^0, q_i^{\mathrm{K}}, \dot{q}_i^{\mathrm{K}}) \triangleq \begin{bmatrix} \Delta(q_i^{\mathrm{K}})\, \dot{q}_i^{\mathrm{K}} - \dot{q}_i^0 \\ q_i^{\mathrm{K}} - q_i^0 \end{bmatrix} = 0 \tag{12}$$

to represent the states continuity through impact dynamics on the edge $\mathcal{S}_i$, where $\Delta(\cdot)$ maps the pre-impact velocity $\dot{q}_i^{\mathrm{K}}$ to its post-impact term. According to Corollary 1 in [17], and the mapping $\alpha_{\mathrm{r}} = \mathcal{M}\alpha_{\mathrm{f}}$, we can then obtain periodic solutions to the quadrupedal dynamics.

Path constraints. In practice, path constraints (inequality constraints) are often used to "fine-tune" the optimal results according to human intuition and physical limitations. Evaluating the optimality of an optimization solution based on experimental performance is rather empirical, and intensive constraint tuning is often needed for field testing. The ultimate target of this paper is to present a method that can be seamlessly used to produce periodic gaits for hardware experiments on sloped terrains. Hence, we explicitly list our path constraints as follows:

- Joint angles do not exceed physical limits;
- Absolute joint velocities below 4 rad/s;
- Absolute acceleration less than 120 rad/s^2;
- Absolute joint torque less than 50 N·m;
- Stepping period $t^{\mathrm{K}} \in [0.29, 0.37]$;
- Nonstance toe's height $\hat{h}_i(q_i^\kappa) \geq 0.1$ at $\kappa = \mathrm{K}/2$;
- Nonstance toe's absolute velocities (parallel to the sloped ground) slower than 1.3 m/s;
- Ground impact velocity $\hat{\dot{h}}_{ns}(q_i, \dot{q}_i) \in [-2, -0.2]$.

Remark that these constraints setup are not modified throughout the optimization for all of the gaits that are experimentally tested in Sec. IV.

Trajectory optimization. Denote the decision variables as $\vartheta^\kappa = \{x_i^\kappa, \dot{x}_i^\kappa, z_i^\kappa, \dot{z}_i^\kappa, z_j^\kappa, \dot{z}_j^\kappa, u_i^\kappa, u_j^{\mathbf{Z},\kappa}\}$ on the node κ. The optimization problem is given as:

$$\min_{\{\vartheta^\kappa\}_{\kappa=0,\ldots\mathrm{K}}} \quad \sum_\kappa \left\| \dot{\xi}_{\mathrm{f}}^\kappa \right\|_2^2 \qquad \kappa = 0, 1 \ldots \mathrm{K} \tag{13}$$

$$\begin{aligned} \text{s.t.} \quad & (C.1)\ \text{dynamic collocation constraints} \\ & (C.2)\ \text{periodic constraints} \\ & (C.3)\ \text{path constraints} \\ & (C.4)\ \text{feasibility constraints} \end{aligned}$$

where $\mathrm{K} = 5$, and the constrains are described above.

Optimal gaits on slopes. By only changing the slope angles to $\phi = 0^\circ, 13^\circ, 15^\circ, 20^\circ, 25^\circ$ in the optimization problem (13), we were able to generated periodic solutions efficiently. These solutions are further used to obtain quadrupedal gaits for experiments. We hereby report the average computational time for all five gaits are 9.7 seconds and 271 searching iterations on a Ubuntu 16.04 machine with Intel Core i7-6820 HQ CPU @ 2.7 GHz with 16 GB RAM. The phase portrait of the gaits on the 13° and $20^\circ \sim 25^\circ$ sloped terrains are shown in solid lines in Fig. 3.

IV. Simulation Validation and Experiments

Before directly enabling these sloped walking gaits optimized by the CCS optimization framework on the actual hardware — a 44 kg, 56 cm wide robot (Fig. 1) — we first validate their physical feasibility and dynamic stability under a feedback control law in a physics engine, RaiSim [19]. The particular control law we chose is a time-based PD approximation of the input-output linearizing controller that track the optimized trajectories, namely the control inputs of the rotational joints are given by

$$u(q, \dot{q}, t) = k_p(\theta^a - y^d(t, (\alpha_{\mathrm{f}}, \alpha_{\mathrm{r}})) + k_d(\dot{\theta}^a - \dot{y}^d(t, (\alpha_{\mathrm{f}}, \alpha_{\mathrm{r}})) \tag{14}$$

where $\theta^a = (\theta_{\mathrm{f}}^\top, \theta_{\mathrm{r}}^\top)^\top$, $k_p, k_d \in \mathbb{R}^{12\times 12}$ are the PD gains, respectively, and y^d are the desired outputs for the quadruped. The theoretical validity of this implementation has been justified using input-to-state stability in [24].

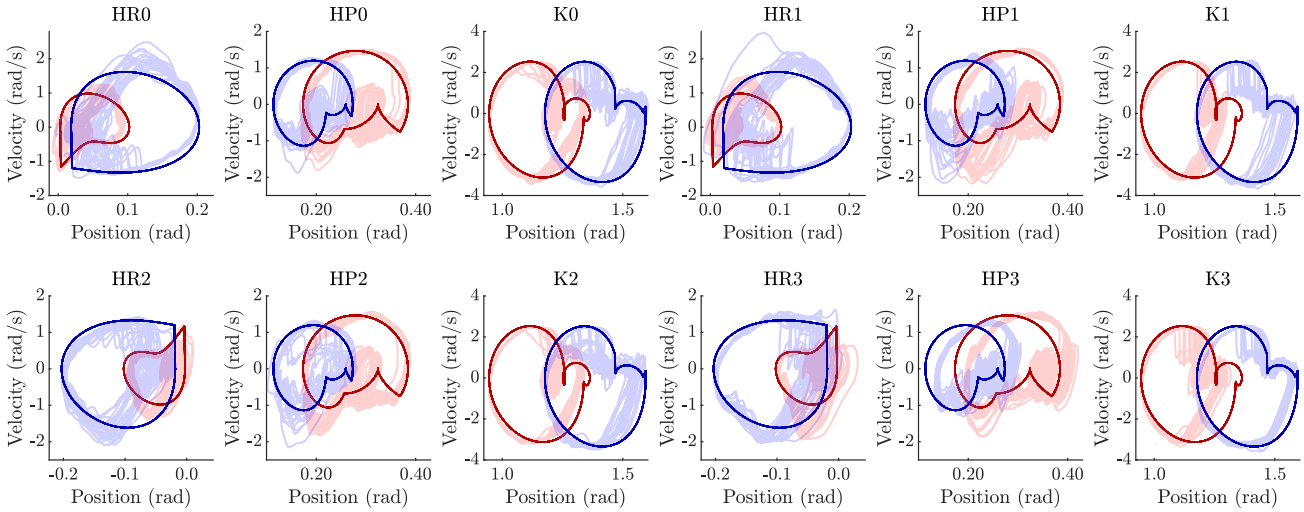

Fig. 3: Phase portraits of the designed gaits (solid lines) vs. experimental data (transparent overlay) for quadrupedal walking on 13° (red) and 20° ∼ 25° (blue) slopes. HR, HP, K are short for hip roll, hip pitch and knee, accordingly.

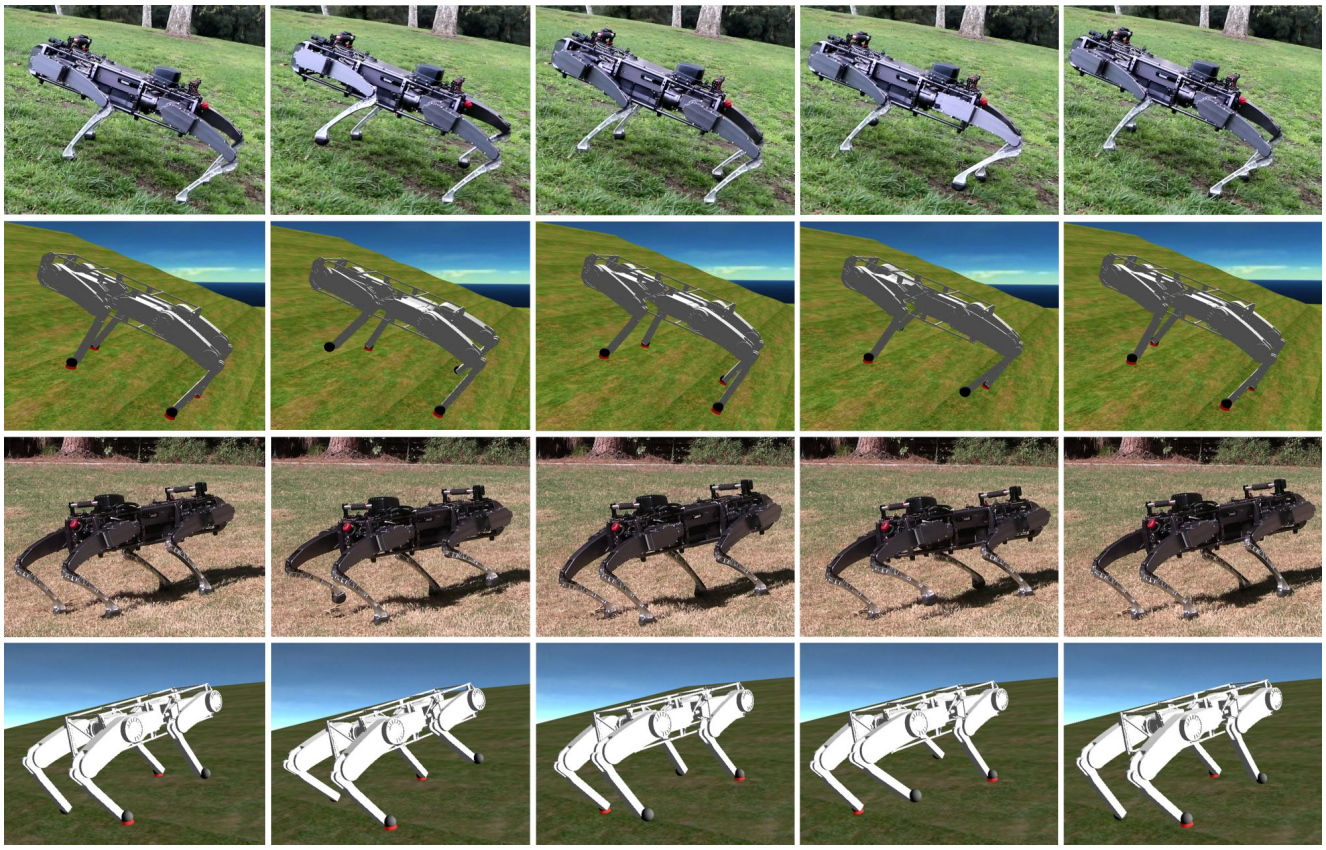

Fig. 4: Full steps of gait tiles for the Vision 60 ambling in outdoor grasslands. The top two is comparison between simulation and experiments for a 13° slope. The bottom two are for walking on a ramp with varying slopes of 20° ∼ 25°.

The quadrupedal robot was first tested on a consistently graded 13° grassy slope with minimal surface variation, which was replicated in RaiSim by creating a plane of constant incline. In order to truly test this methodology, the quadruped was next asked to traverse a grassy slope just after it had rained with inclination ranging from 20° to 25°. In order to emulate the varying slope in RaiSim, a terrain was created with a sinusoidally oscillating height varying between 20° and 25° with a frequency that approximated that of the outdoor environment. As a baseline, both a level-ground gait based controller and the stock controller were tested on the 20° ∼ 25° slope – we report that

neither of which were able to navigate on the sloped terrain successfully. As can be seen in the gait tiles in Fig. 4, our proposed method allows the robot to successfully amble across both the 13° slope and the 20° and 25° slope despite the unmodeled variation in slope and lowered friction effects. See [25] for a video demonstration of the experimental validation of the quadruped, in which we also showed all five gaits walking on slopes of $0^\circ, 13^\circ, 15^\circ, 20^\circ, 25^\circ$ in RaiSim. This result demonstrates the necessity of designing optimal trajectory and controllers based on the specific terrain types using the full-body dynamics. Additionally, we remark that the PD gains and ground friction coefficient are the same across all simulation and experimental implementations.

In addition, we logged 20 seconds of experimental data, and compared them with the desired ambling gait designed by the optimization, as seen in Fig. 3 with phase portraits. Note the difference in the desired behavior for the two terrains. This diversity of behavior further motivates the use of unique gaits conditioned on the terrain to ensure the stability of the robotic system. An important metric to quantify control performance for locomotion is the mechanical cost of transport (MCOT), which was calculated using equation (16) of [14]. Unlike the traditional formulation where the distance term only accounts for the horizontal displacement [1], we used the averaged three-dimensional velocity on the sloped terrain, which also considers the vertical displacement. We report that in simulation, the MCOT for 13° and $20^\circ \sim 25^\circ$ sloped ambling are 2.01 and 2.86, accordingly.

V. Concluding Remarks

In this paper, we extended the method of coupled control systems to generate quadrupedal locomotion on sloped terrains. We started from modelling, in order to theoretically analyze the decoupled dynamics on slopes for the isolated bipedal robots. Then we presented a detailed optimization algorithm used to rapidly generate walking gaits on leve ground and four slopes. The experiments of the Vision 60 robot walking on slopes of 13° and $20 \sim 25^\circ$ demonstrated the scalability of the suggested method towards outdoor locomotion. The future works includes justifying energy efficiency for walking on sloped terrains, incorporating the vision system into the feedback loop to automatically detect the slope angle for on-board gait generation, navigation, and achieving trotting gaits on sloped terrains.

References

[1] S. Collins, A. Ruina, R. Tedrake, and M. Wisse, "Efficient bipedal robots based on passive-dynamic walkers," *Science*, vol. 307, no. 5712, pp. 1082–1085, 2005.

[2] J. Reher, W.-L. Ma, and A. D. Ames, "Dynamic walking with compliance on a cassie bipedal robot," *2019 18th European Control Conference (ECC)*, pp. 2589–2595, 2019.

[3] K. Sreenath, H.-W. Park, I. Poulakakis, and J. W. Grizzle, "Compliant hybrid zero dynamics controller for achieving stable, efficient and fast bipedal walking on MABEL," *The International Journal of Robotics Research*, vol. 30, no. 9, pp. 1170–1193, Aug. 2011.

[4] M. Raibert, K. Blankespoor, G. Nelson, and R. Playter, "Bigdog, the rough-terrain quadruped robot," *IFAC Proceedings Volumes*, vol. 41, no. 2, pp. 10 822 – 10 825, 2008, 17th IFAC World Congress.

[5] A. De and D. E. Koditschek, "Vertical hopper compositions for preflexive and feedback-stabilized quadrupedal bounding, pacing, pronking, and trotting," *The International Journal of Robotics Research*, vol. 37, no. 7, pp. 743–778, 2018.

[6] M. Hutter, C. Gehring, D. Jud, A. Lauber, C. D. Bellicoso, V. Tsounis, J. Hwangbo, K. Bodie, P. Fankhauser, M. Bloesch, R. Diethelm, S. Bachmann, A. Melzer, and M. Hoepflinger, "Anymal - a highly mobile and dynamic quadrupedal robot," in *2016 IEEE/RSJ International Conference on Intelligent Robots and Systems (IROS)*, Oct 2016.

[7] C. Boussema, M. J. Powell, G. Bledt, A. J. Ijspeert, P. M. Wensing, and S. Kim, "Online gait transitions and disturbance recovery for legged robots via the feasible impulse set," *IEEE Robotics and Automation Letters*, vol. 4, no. 2, pp. 1611–1618, April 2019.

[8] C. Gehring, C. D. Bellicoso, S. Coros, M. Bloesch, P. Fankhauser, M. Hutter, and R. Siegwart, "Dynamic trotting on slopes for quadrupedal robots," in *2015 IEEE/RSJ International Conference on Intelligent Robots and Systems (IROS)*, Sep. 2015, pp. 5129–5135.

[9] S. Kajita, F. Kanehiro, K. Kaneko, K. Yokoi, and H. Hirukawa, "The 3d linear inverted pendulum mode: a simple modeling for a biped walking pattern generation," in *2001 IEEE/RSJ International Conference on Intelligent Robots and Systems (IROS).*, vol. 1, 2001, pp. 239–246 vol.1.

[10] M. H. Raibert, B. H. Brown, M. Chepponis, J. Koechling, J. Hodgins, D. Dustman, K. W. rennan, D. Barrett, C. Thompson, J. Hebert, W. Lee, and L. Borvansky, "Dynamically stable legged locomotion (september 1985-septembers1989)," pp. 49–77, 1989.

[11] K. Galloway, K. Sreenath, A. D. Ames, and J. W. Grizzle, "Torque saturation in bipedal robotic walking through control Lyapunov function-based quadratic programs," *IEEE Access*, vol. 3, pp. 323–332, 2015.

[12] J. Reher, E. A. Cousineau, A. Hereid, C. M. Hubicki, and A. D. Ames, "Realizing dynamic and efficient bipedal locomotion on the humanoid robot DURUS," in *IEEE International Conference on Robotics and Automation (ICRA)*, 2016.

[13] W.-L. Ma, S. Kolathaya, E. R. Ambrose, C. M. Hubicki, and A. D. Ames, "Bipedal robotic running with durus-2d: Bridging the gap between theory and experiment," in *Proceedings of the 20th International Conference on Hybrid Systems: Computation and Control*, ser. HSCC '17. New York, NY, USA: ACM, 2017, pp. 265–274.

[14] W. Ma, Y. Or, and A. D. Ames, "Dynamic walking on slippery surfaces : Demonstrating stable bipedal gaits with planned ground slippage," in *2019 International Conference on Robotics and Automation (ICRA)*, May 2019, pp. 3705–3711.

[15] H. Zhao, J. Horn, J. Reher, V. Paredes, and A. D. Ames, "First steps toward translating robotic walking to prostheses: a nonlinear optimization based control approach," *Autonomous Robots*, 2016.

[16] W.-L. Ma and A. D. Ames, "From bipedal walking to quadrupedal locomotion: Full-body dynamics decomposition for rapid gait generation," *International Conference on Robotics and Automation*, 2020.

[17] W. Ma, N. Csomay-Shanklin, and A. D. Ames, "Coupled control systems: Periodic orbit generation with application to quadrupedal locomotion," *IEEE Control Systems Letters*, vol. 5, no. 3, pp. 935–940, 2021.

[18] K. A. Hamed, V. R. Kamidi, W.-L. Ma, A. Leonessa, and A. D. Ames, "Hierarchical and safe motion control for cooperative locomotion of robotic guide dogs and humans: A hybrid systems approach," *arXiv preprint arXiv:1904.03158*, 2019.

[19] J. Hwangbo, J. Lee, and M. Hutter, "Per-contact iteration method for solving contact dynamics," *IEEE Robotics and Automation Letters*, vol. 3, no. 2, pp. 895–902, 2018.

[20] J. W. Grizzle, C. Chevallereau, R. W. Sinnet, and A. D. Ames, "Models, feedback control, and open problems of 3D bipedal robotic walking," *Automatica*, vol. 50, no. 8, pp. 1955 – 1988, 2014. [Online]. Available: http://dx.doi.org/10.1016/j.automatica.2014.04.021

[21] W.-L. Ma, K. Akbari Hamed, and A. D. Ames, "First steps towards full model based motion planning and control of quadrupeds: A hybrid zero dynamics approach," in *2019 IEEE International Conference on Intelligent Robots and Systems (IROS)*, Macau, China, 2019.

[22] A. Hereid, C. M. Hubicki, E. A. Cousineau, and A. D. Ames, "Dynamic humanoid locomotion: A scalable formulation for HZD gait optimization," *IEEE Transactions on Robotics*, 2018.

[23] A. V. Rao, "A survey of numerical methods for optimal control," *Advances in the Astronautical Sciences*, 2009.

[24] S. Kolathaya, "Local stability of pd controlled bipedal walking robots," *Automatica*, vol. 114, p. 108841, 2020.

[25] Experimental video of Vision 60, https://youtu.be/uJedboyzDjc.